



## Functional MRI study with conductivity signal changes during visual stimulation

Hyug-Gi Kim<sup>a</sup>, Youngeun Yoon<sup>b</sup>, Mun Bae Lee<sup>c</sup>, Jeongin Jeong<sup>b</sup>, Jiyoong Lee<sup>b</sup>, Oh In Kwon<sup>c</sup>, Geon-Ho Jahng<sup>d,\*</sup>

<sup>a</sup> Department of Radiology, Kyung Hee University Hospital, Dongdaemoon-gu, Seoul, South Korea

<sup>b</sup> Department of Biomedical Engineering, Undergraduate School, College of Electronics and Information, Kyung Hee University, Giheung-gu, Yongin-si, Gyeonggi-do, South Korea

<sup>c</sup> Department of Mathematics, College of Basic Science, Konkuk University, Seoul, Gwangjin-gu, South Korea

<sup>d</sup> Department of Radiology, Kyung Hee University Hospital at Gangdong, Kyung Hee University College of Medicine, Seoul, Gangdong-Gu, South Korea

### ARTICLE INFO

**Keywords:**

Functional MRI

Conductivity signal

MREPT

Visual stimulation

Cerebrospinal fluid (CSF)

### ABSTRACT

**Background:** Although blood oxygen level-dependent (BOLD) functional MRI (fMRI) is a standard method, major BOLD signals primarily originate from intravascular sources. Magnetic resonance electrical properties tomography (MREPT)-based fMRI signals may provide additional insights into electrical activity caused by alterations in ion concentrations and mobilities.

**Purpose:** This study aimed to investigate the neuronal response of conductivity during visual stimulation and compare it with BOLD.

**Materials and methods:** A total of 30 young, healthy volunteers participated in two independent experiments using BOLD and MREPT techniques with a visual stimulation paradigm at 3 T MRI. The first set of MREPT fMRI data was obtained using a multi-echo spin-echo (SE) echo planar imaging (EPI) sequence from 14 participants. The second set of MREPT fMRI data was collected from 16 participants using both a single-echo SE-EPI and a single-echo three-dimensional (3D) balanced fast-field-echo (bFFE) sequence. We reconstructed the time-course Larmor frequency conductivity to evaluate hemodynamics.

**Results:** Conductivity values slightly increased during visual stimulation. Activation strengths were consistently stronger with BOLD than with conductivity for both SE-EPI MREPT and bFFE MREPT. Additionally, the activated areas were always larger with BOLD than MREPT. Some participants also exhibited decreased conductivity values during visual stimulations. In Experiment 1, conductivity showed significant differences between the fixation and visual stimulation blocks in the secondary visual cortex (SVC) and cuneus, with conductivity differences of 0.43 % and 0.47 %, respectively. No significant differences in conductivity were found in the cerebrospinal fluid (CSF) areas between the two blocks. In Experiment 2, significant conductivity differences were observed between the two blocks in the SVC, cuneus, and lingual gyrus for SE-EPI MREPT, with differences of 0.90 %, 0.67 %, and 0.24 %, respectively. Again, no significant differences were found in the CSF areas.

**Conclusion:** Conductivity values increased slightly during visual stimulation in the visual cortex areas but were much weaker than BOLD responses. The conductivity change during visual stimulation was less than 1 % compared to the fixation block. No significant differences in conductivity were observed between the primary visual cortex (PVC)-CSF and SVC-CSF during fixation and visual stimulations, suggesting that the observed conductivity changes may not be related to CSF changes in the visual cortex but rather to diffusion changes.

**Abbreviations:** 3D, three-dimensional; BFFE, balanced fast-field-echo; BOLD, blood oxygen level-dependent; CSF, cerebrospinal fluid; DHb, deoxyhemoglobin; Exp, Experiment; fMRI, functional MRI; HFC, high-frequency conductivity; MREIT, magnetic resonance electrical impedance tomography; MREPT, magnetic resonance electrical properties tomography; PVC, primary visual cortex; ROI, Regions-of-interest; RF, radio-frequency; SE-EPI, spin-echo echo-planar-imaging; SVC, secondary visual cortex; T1W, T1-weighted.

\* Correspondence to: Department of Radiology, Kyung Hee University Hospital at Gangdong, Kyung Hee University College of Medicine, 892 Dongnam-ro, Seoul, Gangdong-Gu 05278, South Korea.

E-mail address: [ghjahng@gmail.com](mailto:ghjahng@gmail.com) (G.-H. Jahng).

<https://doi.org/10.1016/j.jneumeth.2024.110288>

Received 3 June 2024; Received in revised form 27 August 2024; Accepted 12 September 2024

Available online 19 September 2024

0165-0270/© 2024 Elsevier B.V. All rights are reserved, including those for text and data mining, AI training, and similar technologies.

Future research should explore the potential of MREPT to detect neuronal electrical activity and hemodynamic changes, with further optimization of the MREPT technique.

### Major Contribution to the Field

The major contribution of this study is the demonstration of the feasibility and limitations of using Magnetic Resonance Electrical Properties Tomography (MREPT) to measure neuronal activity changes during visual stimulation in the human brain. Unlike the traditional BOLD fMRI, which primarily reflects changes in blood oxygenation, MREPT provides insights into the electrical properties of brain tissues, specifically conductivity changes associated with neuronal activation. This novel approach could offer a complementary perspective to BOLD fMRI, potentially enhancing our understanding of the complex physiological processes underlying brain function.

### Key Findings

**1. Conductivity Changes During Visual Stimulation:** The study found that conductivity values slightly increased during visual stimulation in the visual cortex areas. However, these changes were significantly smaller than those observed with BOLD fMRI, with conductivity changes being less than 1 % during visual stimulation compared to the fixation block. This indicates that while MREPT can detect conductivity changes, its sensitivity is lower than that of BOLD fMRI for mapping brain activation during visual tasks.

**2. CSF Contribution to Conductivity Changes:** The study investigated whether changes in conductivity during visual stimulation were influenced by cerebrospinal fluid (CSF) signals. The results showed no significant differences in conductivity values between fixation and visual stimulation in the CSF areas of the primary visual cortex (PVC-CSF) and secondary visual cortex (SVC-CSF). This suggests that the observed conductivity changes are more likely related to the mobility of charged ions under the influence of electric field changes rather than CSF alterations.

**3. Differences in Activation Patterns Between BOLD and MREPT:** The activation patterns detected by BOLD fMRI were much more robust and extensive compared to those detected by MREPT. BOLD fMRI consistently showed stronger signal changes and larger activated areas during visual stimulation. This disparity highlights the different physiological mechanisms captured by each imaging modality, with BOLD being more sensitive to hemodynamic changes while MREPT captures changes in ion concentration and mobility within the brain tissue.

### 1. Introduction

The blood oxygen level-dependent (BOLD) functional MRI (fMRI) is the most popular functional imaging method for investigating neuronal activity in the brain (Kwong et al., 1992; Ogawa et al., 1992). BOLD is based on measuring the concentration of intravascular deoxyhemoglobin (dHb), and it typically consists of intravascular and extravascular components from both small and large vessels. BOLD signals can be obtained using a gradient-echo (GE) or spin-echo (SE) sequence. Although the SE-based BOLD signal minimizes large vessel signals from intravascular and extravascular contributions, the extent of activation appears to be larger than that of the parenchyma signal (Turner, 2002). Moreover, the interpretation of BOLD signals is typically complicated because BOLD signals come from changes in several physiological parameters, such as cerebral blood flow (CBF), cerebral blood volume (CBV), and oxygen consumption rate (CMRO<sub>2</sub>) (Buxton and Frank, 1997). Both action potential and synaptic activity correlate with the BOLD signal (Heeger et al., 2000; Logothetis et al., 2001), indicating a direct correlation between BOLD signals and the underlying neuronal activity with cellular action potentials.

BOLD fMRI studies have significantly enhanced our understanding of how the human brain processes visual information (Huang et al., 2021). Visual stimulation activates the primary visual cortex (PVC) and the

secondary visual cortex (SVC). The PVC, also known as Brodmann's area 17, is located in the occipital lobe near the calcarine fissure at the back of the brain and is responsible for processing basic visual information (Huang et al., 2021). Surrounding the PVC, the SVC includes Brodmann's areas 18 and 19, which receive signals from the PVC for further analysis and discrimination of visual input, such as motion, complex shapes, and position. The peristriate cortex (Brodmann's area 18) features an inverted visual field receptive topography compared to the striate cortex, while the parastriate cortex (Brodmann's area 19) surrounds area 18, maintaining an identical retinotopic representation (Kotoula et al., 2023; Soares et al., 2016). fMRI studies are increasingly utilized in preoperative planning for brain tumor surgeries located in the visual cortex (Chaudhry et al., 2021; Hense et al., 2021; Lakhani et al., 2023). Additionally, previous fMRI research has examined neurofunctional activations involved in processing visual stimuli from food in individuals with eating disorders (Althubeiti et al., 2022; Celegin et al., 2023). Various machine learning methods have also been developed to analyze neural activities, including brain image functional alignment, brain activity pattern analysis, and visual stimuli reconstruction (Huang et al., 2021; Meng and Ge, 2022). Recently, an fMRI study investigated brain responses to peripheral visual stimulation (Park et al., 2024) and revealed a sub-second activation sequence in the human visual cortex (Wittkuhn and Schuck, 2021). These studies have demonstrated that the visual cortex is organized in a retinotopic manner, creating a spatial map of the visual field on the cortex, and that attention enhances neural responses in visual areas.

The electrical conductivity of biological tissues is determined by several factors, such as cell density, cellular volume fractions, composition and amount of materials, and concentrations and mobility of ions in the cellular fluids (Hancu et al., 2019, 2015). The cellular fluids are conductors through which conductivity values are determined based on the concentrations and mobilities of ions and other mobile charge carriers (Gabriel et al., 2009) expressed in the formula:

$$\sigma = qNM = \sum_i^I q_i N_i M_i \quad (1)$$

where  $\sigma$  is the conductivity,  $q$  represents the charge carried by the ions,  $N$  denotes the number of charged particles per unit volume (also known as concentration), and  $M$  signifies the mobility—the average velocity of a charge carrier when subjected to a unit electric field strength. Thus, conductivity escalates with increasing ion concentrations and ionic mobility. Using MRI, the cerebrospinal fluid (CSF) signal can represent ion concentration and mobility can be represented by diffusion. If neuronal activity increases conductivity, then conductivity in the CSF area in the neuron may be altered. Because previous studies showed that diffusion-based fMRI increased during neuronal stimulations (Le Bihan et al., 2006), the conductivity signal can also be increased during neuronal stimulation.

Magnetic resonance electrical properties tomography (MREPT) produces high-frequency isotropic conductivity ( $\sigma_H$ ) and permittivity ( $\epsilon_H$ ) images at the applied Larmor frequency by generating a radio-frequency (RF) eddy current and measuring an induced RF magnetic field using a B1 mapping method (Gurler and Ider, 2017; Katscher et al., 2009; Leijsen et al., 2021). MREPT signals can typically be acquired with a spin-echo or gradient-echo sequence to obtain both magnitude and phase data, which are sensitive to electromagnetically generated contrasts caused by internal neural sources (Konn et al., 2003). Therefore, MREPT can measure high-frequency tissue electrical properties without injecting any external current into the human body (Katscher et al., 2013). Conductivity imaging using MREPT allows for evaluating in-vivo

physiological information (Hancu et al., 2019, 2015). Because BOLD fMRI signals depend on CBF, CBV, and CMRO<sub>2</sub> altered by local electric synaptic activity, MREPT-based fMRI signals may explain additional information on electric activity caused by alteration of ion concentrations and mobilities.

Although several neural activity studies have been conducted by applying an external injection of electrical current, called magnetic resonance electrical impedance tomography (MREIT) (Miceli et al., 2017; Sadleir et al., 2019, 2017), there have been few studies evaluating neural activities without applying an external current, which is called MREPT. This study aimed to investigate the neuronal response of conductivity during visual stimulation with MREPT techniques and to compare that with BOLD. We performed two independent experiments with BOLD and MREPT techniques using a visual stimulation paradigm at 3 T MRI. MREPT fMRI data were obtained with two different sequences of a multi-echo or single-echo spin-echo-echo planar imaging (SE-EPI) and a single-echo three-dimensional (3D) balanced fast-field-echo (bFFE), which were optimally used to map a high-frequency conductivity (Bieri et al., 2006; Jahng et al., 2021; Katscher and van den Berg, 2017). Moreover, two independent experiments were performed while changing the duration of the visual stimulation, number of stimulation blocks, repetition time (TR), and echo time (TE). In this study, we experimented with a similar voxel resolution for both BOLD and MREPT. We expected increased conductivity due to increasing neural activity in a voxel with visual stimulation caused by alteration of ion concentrations and mobilities. The major contribution of this study is the demonstration of the feasibility and limitations of using MREPT to measure neuronal activity changes during visual stimulation in the human brain. Some papers have been published using low-frequency conductivity changes during electrical stimulation in animal studies. Our study was performed on high-frequency conductivity changes during stimulation in humans. MREPT-based fMRI study is a novel method to enhance our understanding of the complex physiological processes underlying brain function.

## 2. Materials and methods

### 2.1. Participants

Our Institutional Review Board (IRB) approved this cross-sectional prospective study (IRB KHNCMC 2020–03–017), and written informed consent was obtained from all participants. In total, 30 young healthy volunteers were recruited from the local community. None of the volunteers had neurological or psychiatric disease history. All young controls underwent the Korean version of the mini-mental state examination (K-MMSE) test based on global cognitive ability and brain fMRI scans. In this study, we performed two independent experiments. The first experiment was performed on 14 young participants (mean age  $\pm$  standard deviation (SD),  $24.8 \pm 3.5$  years; sex(male/female), 8/6). The second experiment was performed on 16 young participants (mean age  $\pm$  SD,  $24.9 \pm 1.7$  years; sex(male/female), 2/14). The MMSE scores (mean  $\pm$  SD) were  $29.7 \pm 0.8$  for experiment 1 and  $29.7 \pm 0.4$  for experiment 2.

### 2.2. Interface of the visual stimulation

Fig. 1 illustrates the visual stimulation interface. The checkerboard visual stimulation was presented using the nordicAktiva stimulus presentation system (NordicImagingLab, Bergen, Norway). This system includes the SyncBox, which allows users to select how the trigger pulse from the scanner is transferred to the software presenting the stimuli. The SyncBox receives a signal from the MRI scanner and automatically controls the stimulus presentation personal computer. The nordicAktiva stimulus presentation system was interfaced with the high-resolution goggles of the visual system via an interface cable. These goggles are mounted onto the 32-channel head

coil to present stimuli. This binocular goggle visual system can be adjusted to fit the individual well. The participant can provide feedback by pressing one of four buttons on the MR-compatible ResponseGrips, which connect to the interface unit in the operator room.

After acquiring the fMRI data, time-series conductivity maps were calculated from MREPT data using our MathLab code. Structure images, time-series BOLD images, and calculated time-series conductivity maps were then further processed using Statistical Parametric Mapping version 12 software (SPM12; Wellcome Department of Imaging Neuroscience, University College, London, UK). Using SPM12 software, we performed to preprocess of the acquired and calculated time-series images or maps for motion correction, co-registration, spatial normalization, brain tissue segmentation, and Gaussian smoothing. These preprocessed images were then fitted with a general linear model to produce a statistical parametric map with a given statistical threshold. Details of the fMRI paradigms, MRI data acquisition, time-series image conductivity mapping, fMRI data processing, and statistical analyses are explained in the following subsections.

### 2.3. Functional MRI paradigm

Two sets of independent experiments were performed in this study while modifying the length of stimulation duration and the number of stimulation blocks with different imaging sequences for MREPT data. The paradigm with visual stimulation was used for both experiments, although with different block designs. Both experiments had fixation and stimulation blocks. A cross-sign was used for the fixation or baseline condition, but a black-and-white checkerboard was used for the visual stimulation condition. The model paradigm was presented using the Nordic fMRI system (NordicImagingLab, Bergen, Norway). Supplementary Fig. S2 shows the paradigms for both experiments for the three different sequences of 3D bFFE, BOLD, and SE-EPI. We also scanned the structure imaging sequences of 3D T1-weighted imaging (3D T1WI), T2-weighted imaging (T2WI), and fluid-attenuated inversion recovery (FLAIR) imaging between the fMRI scan.

In the first experiment (Supplementary Fig. S2.A.Exp1), both the BOLD and two-echo SE-EPI MREPT fMRI sequences were run with three fixation and three stimulation blocks. BOLD fMRI was performed with 30 s per block, 15 scans per block, and 90 vol scans. The running time was 3 min 0 s. For MREPT, the multi-echo (me) SE-EPI sequence was used. The me-SE-EPI fMRI was run with 60 s per block, 10 scans per block, and 60 vol scans. The running time was 6 min 0 s. The detailed stimulation paradigms are summarized in Supplementary Table S1.

In the second experiment (Supplementary Fig. S2.B.Exp2), we replaced two-echo SE-EPI with one-echo SE-EPI for MREPT and added a single-echo 3D bFFE sequence for MREPT. All three fMRI sequences were run with two fixation and two stimulation blocks. BOLD fMRI was performed with 30 s per block, 15 scans per block, and 60 vol scans. The running time was 2 min 0 s. For MREPT, the single-echo SE-EPI fMRI was run with 60 s per block, 30 scans per block, and 120 vol scans. The running time was 4 min 0 s. The single-echo 3D bFFE fMRI was run with 90 s per block, 15 scans per block, and 60 vol scans. The running time was 6 min 0 s. Supplementary Table S1 also summarizes the detailed information.

### 2.4. MR data acquisitions

The fMRI study was performed on a 3 T MRI System (Ingenia, Philips Medical System, Best, the Netherlands) with a 32-channel phase-array sensitivity-encoding (SENSE) coil. First, the GE-EPI sequence was run to obtain BOLD signals for both experiments. The scan durations were 3 minutes for experiment 1 and 2 minutes for experiment 2. The detailed scan parameters are listed in Supplementary Table S1. Second, the SE-EPI sequence was run to obtain both magnitude and phase to then calculate the high-frequency conductivity for each dynamic scan point. The number of echoes was two for the first experiment and one for the

second experiment. The detailed scan parameters are also listed in [Supplementary Table S1](#). Third, the sagittal 3D bFFE sequence was run to obtain both magnitude and phase to then calculate the high-frequency conductivity for each dynamic scan point. The detailed acquisition parameters are summarized in [Supplementary Table S1](#). For image registration, sagittal structural 3D T1-weighted (3D T1W) images were acquired with the turbo field echo sequence with a 1 mm isotropic voxel. Finally, T2W turbo-spin-echo and FLAIR images were acquired to evaluate any brain abnormalities.

## 2.5. Conductivity mapping for both spin-echo and 3D bFFE MREPT scans

The time-harmonic electric and magnetic fields,  $\mathbf{E}$  and  $\mathbf{B}$ , satisfy

$$\nabla \times \mathbf{E} = -i\omega\mu_0\mathbf{B} \text{ and } \nabla \times \mathbf{B} = \kappa\mathbf{E}$$

where  $\omega$  is the angular frequency,  $\mu_0 = 4\pi \times 10^{-7} \text{ N/A}^2$  is the magnetic permeability of the free space, and  $\kappa$  is the admittivity. At a high frequency (Larmor frequency), the electrical tissue properties of conductivity  $\sigma_H$  and permittivity  $\epsilon_H$  satisfy

$$\nabla^2 \mathbf{B}_1 = i\omega\mu_0\tau_H \mathbf{B}_1 - \frac{\nabla\tau_H}{\tau_H} \times (\nabla \times \mathbf{B}_1) \quad (1')$$

where  $\mathbf{B}_1$  is the B1 field and  $\tau_H = \sigma_H + i\omega\epsilon_H$  ([Katscher et al., 2009](#)). We have ignored changes in the relative permeability because they are considered to be negligible for biological tissues ([Collins et al., 2002](#)). Thus, the magnetic permeability of tissue is set to that of the free space. The transverse field of  $\mathbf{B}_1$  can be decomposed into the positively rotating field  $B_1^+ = \frac{1}{2}(B_x + iB_y)$  and the negatively rotating field  $B_1^- = \frac{1}{2}(B_x - iB_y)$ . We denoted  $\phi^+$  and  $\phi^-$  as the phase terms of  $B_1^+$  and  $B_1^-$ , respectively. By assuming  $\sigma_H \gg \omega\epsilon_H$ , a phase-based MREPT formula for reconstructing the conductivity was derived as:

$$\left( \nabla\phi^r \cdot \nabla \left( \frac{1}{\sigma_H} \right) \right) + \frac{\nabla^2\phi^r}{\sigma_H} - 2\omega\mu_0 = 0 \quad (2)$$

where  $\phi^r = \phi^+ + \phi^-$  is the measurable transceive phase using MRI ([Gurler and Ider, 2017](#)). This partial differential equation is sensitive to the measured noise. Therefore, to stabilize the formula [2], the MREPT formula based on a convection reaction equation can be derived by adding the regularization coefficient  $c$ .

$$-c\nabla^2 \left( \frac{1}{\sigma_H} \right) + \left( \nabla\phi^r \cdot \nabla \left( \frac{1}{\sigma_H} \right) \right) + \frac{\nabla^2\phi^r}{\sigma_H} = 2\omega\mu_0 \quad (3)$$

To solve the convection reaction partial differential equation [3], we used the 2-dimensional finite-difference method. The phase image of each dynamic time-point was processed to map the high-frequency conductivity map for both MREPT fMRI data acquired with SE-EPI and 3D bFFE sequences. The time-series conductivity maps were calculated without applying the background noise removal technique.

## 2.6. fMRI data processing

Statistical parametric mapping version 12 software (SPM12; Wellcome Department of Imaging Neuroscience, University College, London, UK) was used for data preprocessing and voxel-based statistical analysis. First, BOLD, SE-EPI, and/or 3D bFFE functional images of each sequence for each participant were realigned to the first volume to minimize the effect of head motion during the brain scan, and a mean volume image was created for each sequence. Information on the subject's motion was used as the regressor during the individual-level analysis. The dynamic MREPT conductivity maps from SE-EPI and/or 3D bFFE were also realigned according to the corresponding magnitude images. Second, the mean volume image for each sequence was co-registered to the corresponding structural 3D T1WI; therefore, all functional images and dynamic conductivity maps were also co-registered to the 3D T1WI.

Third, 3DT1WI for each participant was spatially normalized onto the standard Montreal Neurological Institute (MNI) brain template by using nonlinear transformations. Both BOLD and dynamic conductivity functional images were also spatially normalized into the standard brain template using the deformation field information of the 3D T1W. Finally, Gaussian smoothing using a full-width at half maximum (FWHM) of  $7 \times 7 \times 7 \text{ mm}^3$  for the BOLD and  $12 \times 12 \times 12 \text{ mm}^3$  for others was performed for the voxel-based statistical analysis. These analysis steps were repeated separately in two different experiments.

## 2.7. Statistical analyses

### 2.7.1. Voxel-based analyses

For the individual level (first-level) analysis, the activation maps with visual stimulation were generated using a voxel-based general linear model (GLM) approach ([Friston et al., 1994](#)) while comparing the fixation condition for each session, each sequence, and each participant. Therefore, two contrast maps—activation and deactivation maps—were generated for each session of each sequence. We used the significance level of  $p < 0.001$  without correcting for multiple comparisons, and the extent threshold was 50 voxels.

For the group-level (second-level) analysis, the two contrast maps obtained from the individual-level analyses were used to investigate the average of all participants for each sequence using the one-sample  $t$ -test. The activated or deactivated map during visual stimulation against the fixation was identified with a significance level of  $p < 0.05$  while correcting for multiple comparisons using a false discovery rate (FDR), and the extent threshold was 50 voxels. These analysis steps were separately repeated in two different experiments. To identify anatomical areas of the activated or deactivated brain, the  $t$ -test results were standardized into Talairach coordinate using the GingerALE and Talairach Client software (University of Texas Health Science Center San Antonio, UTHSCSA).

### 2.7.2. Regions-of-interest (ROI)-based analyses

The ROIs were placed by selecting atlas-based areas. The four atlas-based ROIs for both experiments were defined at the primary visual cortex (PVC, BA17), secondary visual cortex (SVC, BA 18 and 19), cuneus, and lingual gyrus. In addition, we masked cerebrospinal fluid (CSF) areas in the PVC and SVC by the multiplication of the CSF tissue map obtained from the segmentation of 3D T1WI by PVC (called PVC\_CSF) or SVC (called SVC\_CSF) ROI areas for both experiments to evaluate CSF signal contributions in BOLD and conductivity. Average signal values for each participant, each dynamic scan, and each sequence were obtained from each masked area.

We obtained time-course signal intensities and conductivity values from each ROI, each sequence, and each participant. To normalize individual time-course signal intensities for each ROI, we divided the individual time-course signal intensity for each time point according to the mean fixation signal intensity. To calculate the percent difference of signal changes between two conditions for each ROI and each sequence, we calculated mean signal intensities during the visual stimulation. The average percent signal changes between the two conditions were then calculated by  $\frac{\Delta S}{S(\%)} = (\bar{S}_v - \bar{S}_f) \times 100\% / \bar{S}_f$ , where  $\bar{S}_v$  and  $\bar{S}_f$  are the mean signal intensities during the visual (v) stimulation and fixation (f) conditions, respectively. We averaged those values over all subjects for each time course scan.

## 3. Results

### 3.1. Representative activation maps during the visual stimulation for BOLD and MREPT

[Figure S3](#) presents representative single-slice, single-time point images of BOLD and both the magnitude and conductivity of

MREPT from experiments 1 (A.Exp 1) and 2 (B.Exp 2). The conductivity maps were of reasonable quality.

**Fig. 1** displays representative activation maps during visual stimulation for BOLD and MREPT with SE-EPI and bFFE for experiments 1 (A. Exp1) and 2 (B.Exp2) from four independent participants. Conductivity values showed a slight increase during visual stimulation (red color). The activation strengths were consistently stronger with BOLD than conductivity for both SE-EPI MREPT and bFFE MREPT. Additionally, the activated areas were always larger with BOLD than with MREPT.

### 3.2. Signal changes during the visual stimulation for BOLD and MREPT

**Fig. 2** illustrates BOLD signal changes and conductivity changes during the time-course scans for the four participants shown in **Fig. 1**. BOLD signal increased during the visual stimulation due to increasing CBV, CBF, and CMRO<sub>2</sub> as expected. Conductivity values showed significant variation during visual stimulation in participants S01 and S12 acquired by SE-EPI MREPT, and participant S23 acquired by bFFE.

Supplementary Figures S4 and S5 show the two-dimensional activation maps during visual stimulation for MREPT (**S4A and S5A**) and BOLD (**S4B and S5B**) obtained by each participant for experiments 1 and 2, respectively. Furthermore, decreased conductivity values were observed during visual stimulations in a few participants, as shown in Supplementary Figure S6. While increased conductivity is generally expected during neural activation, the decreased conductivity observed in some participants suggests complex underlying mechanisms, including inhibitory neural processes, individual variability, and localized hemodynamic changes.

### 3.3. Averaged BOLD and conductivity signal changes during the visual stimulation at the PVC and SVC

**Fig. 3** presents the averaged signal changes over all participants during visual stimulation for BOLD and conductivity with SE-EPI MREPT and/or 3D bFFE MREPT for experiments 1 (A.Exp1) and 2 (B. Exp2), obtained from the PVC and SVC ROI areas. The BOLD and conductivity values (red color) were averaged across all participants. Unlike BOLD signal changes, conductivity values did not significantly increase during visual stimulation as depicted in **Fig. 3**.

**Table 1** summarizes the averaged signal changes and their standard deviations over all participants for the fixation and visual stimulation blocks, along with the paired t-test results between the two stimulation blocks at selected brain areas for experiment 1. BOLD always showed a significant difference between the fixation and visual stimulation blocks for all defined ROIs. Conductivity showed a significant difference between the two blocks at SVC and cuneus, with conductivity differences of 0.43 % and 0.47 %, respectively.

**Table 2** summarizes the averaged signal changes and their standard deviations over all participants for the fixation and visual stimulation blocks, along with the paired t-test results between the two stimulation blocks at selected brain areas for experiment 2. Conductivity showed a significant difference between the two blocks at SVC, cuneus, and lingual gyrus for SE-EPI MREPT, with conductivity differences of 0.90 % for SVC, 0.67 % for cuneus, and 0.24 % for lingual gyrus.

### 3.4. Evaluation of the contribution of CSF signals to BOLD and conductivity changes

**Fig. 4** shows similar results obtained from CSF areas in PVC (PVC-CSF) and SVC (SVC-CSF). CSF signals in BOLD increased during brain activation for experiment 1, but those did not show in experiment 2. CSF signals in conductivity varied a lot and slightly increased during the visual stimulation, but those were not statistically significant.

**Tables 1 and 2** additionally summarize the averaged signal changes and their standard deviations over all participants for the fixation and visual stimulation blocks, along with the paired t-test results between

the two stimulation blocks at selected CSF brain areas for experiments 1 and 2, respectively. In experiment 1, as listed in **Table 1**, BOLD also showed a significant difference between the fixation and visual stimulation blocks for the selected CSF areas at both PVC ( $p<0.0001$ ) and SVC ( $p<0.0001$ ). However, conductivity was not significantly different between the two blocks in the CSF ROIs at both PVC ( $p=0.4709$ ) and SVC ( $p=0.0879$ ). In experiment 2, as listed in **Table 2**, BOLD showed a significant difference between the fixation and visual stimulation blocks for the selected CSF areas at PVC ( $p=0.0029$ ) but not at SVC ( $p=0.1693$ ). In addition, conductivity was not significantly different between the two blocks in the CSF ROIs at PVC with SE-PEI ( $p=0.3302$ ) and bFFE ( $p=0.0973$ ) and SVC with SE-EPI ( $p=0.0898$ ) and bFFE ( $p=0.3453$ ).

## 4. Discussion

Functional MREPT can be influenced by ion concentration and mobility. During neuronal activation, diffusion varies (Le Bihan et al., 2006), and CSF and interstitial fluid (ISF) signals can also change in the extracellular area due to restricted proton mobility from cell swelling during neuronal stimulation. The functional MREPT signal simultaneously reflects the electrical properties of both extra- and intra-cellular activity and can depend on changes in the total ion concentration in the voxel during stimulation. This complexity makes understanding the physiology of neuronal changes in the brain challenging. The goal of this study was to investigate the neuronal response of conductivity during visual stimulation using MREPT techniques and compare it with BOLD. We hypothesized that conductivity would increase during neural activity due to alterations in ion concentrations and mobilities. However, we found that conductivity increased only slightly during visual stimulation in visual cortex areas and was much weaker than BOLD (Tables 1 and 2, Fig. 1). This section discusses three key points: 1) differences in neuronal activation detected by conductivity versus BOLD, 2) the contribution of CSF to conductivity changes during neuronal activation, and 3) other parameters related to conductivity-based fMRI. Finally, we address some difficulties and limitations of conductivity-based fMRI.

### 4.1. Differences in neuronal activation detected by conductivity versus BOLD

In this study, BOLD was found to be much more sensitive in mapping brain activation during visual stimulation than conductivity measured by MREPT. The conductivity change during visual stimulation was less than 1 % compared to the fixation block. Additionally, some participants did not show brain activation by MREPT during visual stimulation, indicating minimal conductivity change during brain activation. BOLD signals depend on R2\* changes, while conductivity is measured through phase changes. Strong BOLD signals but weak conductivity changes during visual stimulation suggest larger signals from R2\* changes. This is expected, as BOLD signals originate from blood vessels, unlike conductivity signals which depend on ion concentrations and mobility. BOLD changes reflect hemodynamics, whereas conductivity can change due to both hemodynamics and neuronal activity. Previous studies have shown that hemodynamic changes affect Bz data in the brain (Luo et al., 2009). Ionic currents from visual activity minimally affect phase signals at 3 T MRI. Most magnitude changes stem from BOLD effects with multiple frequency offsets within a voxel, while phase changes are measurable by in-phase frequency offsets. Conductivity changes might relate to extracellular ion concentrations and diffusion induced by neuronal activity, causing phase dispersion and magnitude changes (Le Bihan et al., 2006; Truong et al., 2006). Since this study did not include diffusion-based fMRI results, further research should investigate the source of conductivity changes during neuronal activation by combining diffusion-based and conductivity-based fMRI studies.

BOLD signals arise from blood vessels, with blood conductivity around 0.67 S/m affecting conductivity contrast with blood flow. In static conditions, BOLD and conductivity increase with blood flow or

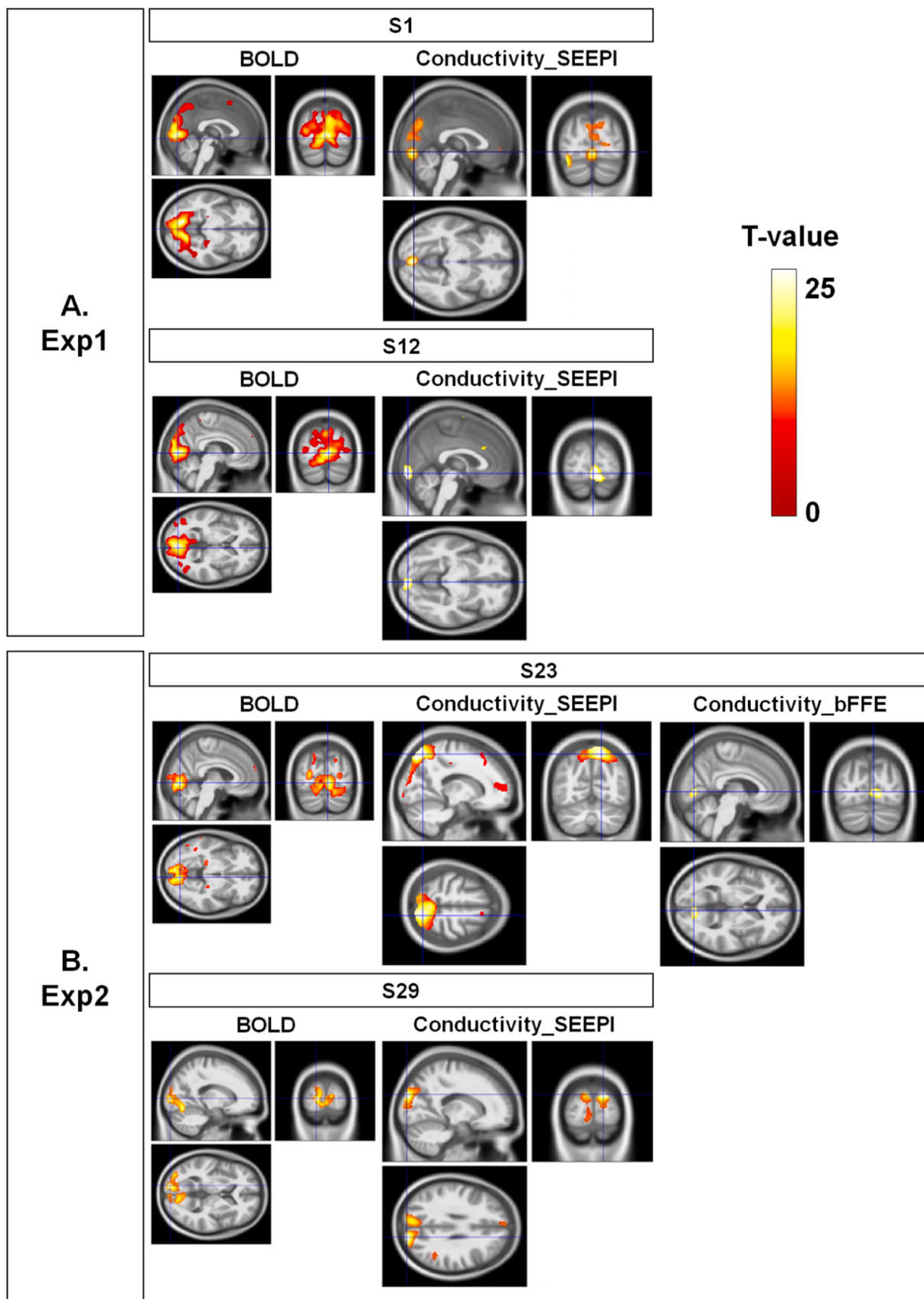
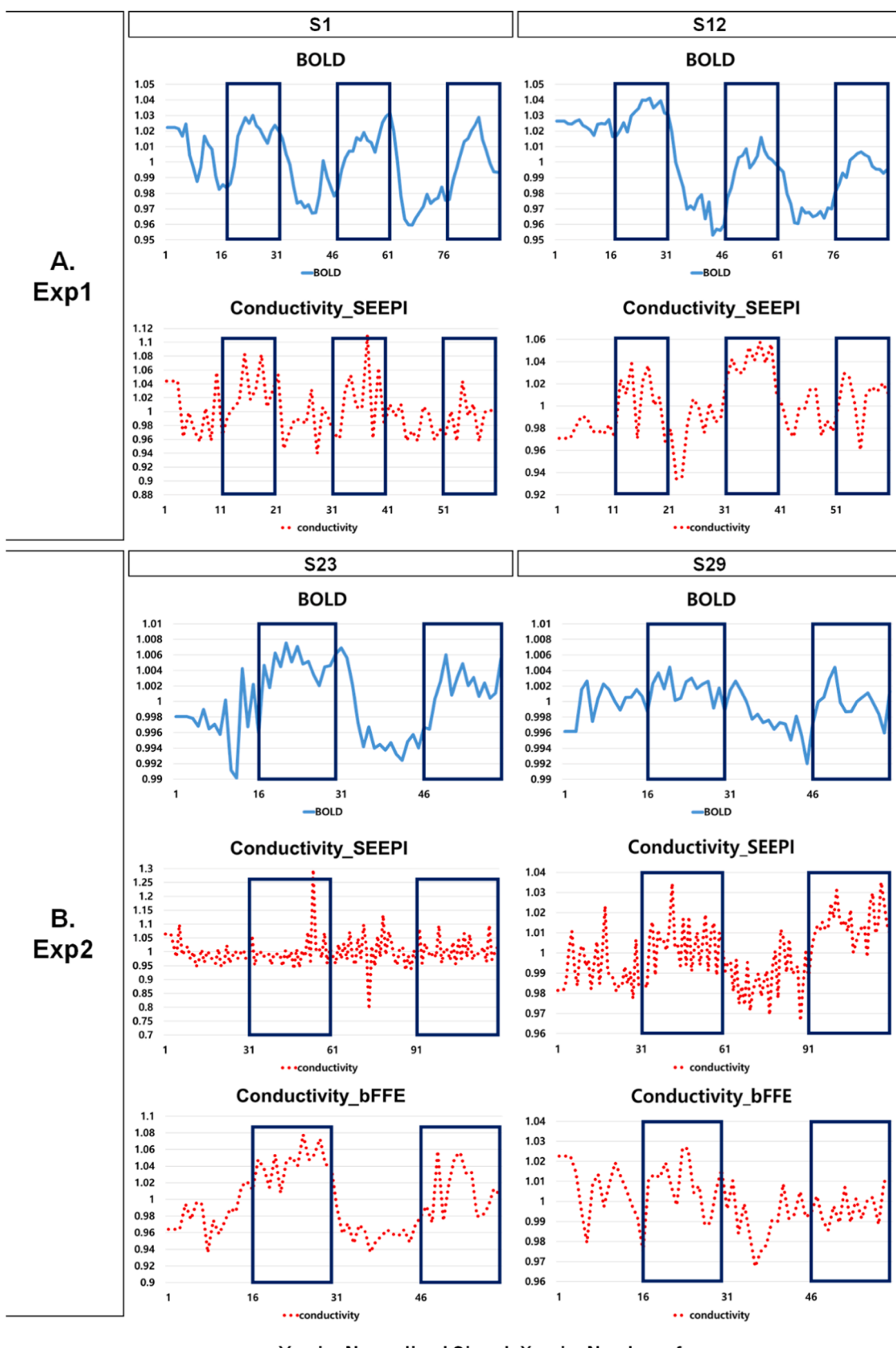
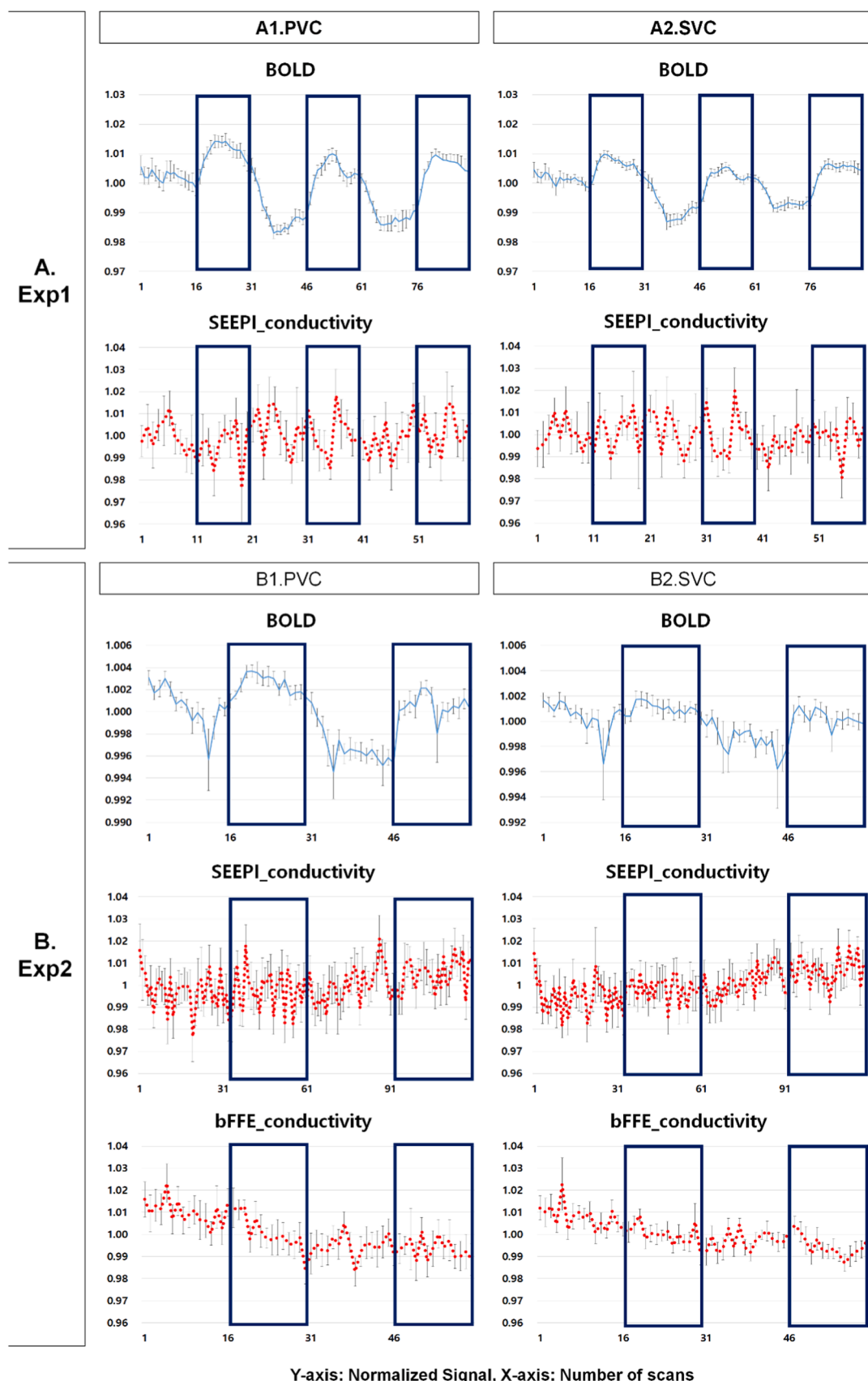


**Fig. 1.** Representative activation maps during the visual stimulation for BOLD and MREPT with spin-echo echo-planar imaging (SEEPI) and three-dimensional balanced fast-field-echo (bFFE) for experiments 1 (A. Exp1) and 2 (B. Exp2) from four independent participants. The conductivity values were slightly increased during visual stimulation (red color). Abbreviations: Exp1, experiment 1; Exp2, experiment 2; S##, subject's number ##; BOLD, blood oxygen level dependent.



Y-axis: Normalized Signal, X-axis: Number of scans

**Fig. 2.** Signal changes during the visual stimulation for BOLD and MREPT with spin-echo echo-planar imaging (SEEPI) and three-dimensional balanced fast-field-echo (bFFE) for experiments 1 (A. Exp1) and 2 (B. Exp2) activated areas shown in Fig. 1. The conductivity values were slightly increased during visual stimulation (red color). Abbreviations: Exp1, experiment 1; Exp2, experiment 2; S##, subjects with participant's number ##; BOLD, blood oxygen level dependent.



Y-axis: Normalized Signal, X-axis: Number of scans

**Fig. 3.** Averaged signal changes over all participants during the visual stimulation for BOLD and conductivity acquired with spin-echo echo-planar imaging (SEEPI) MREPT and/or three-dimensional balanced fast-field-echo (bFFE) for experiments 1 (A.Exp1) and 2 (B.Exp2) at the primary visual cortex (PVC) and secondary visual cortex (SVC). The values of BOLD and conductivity (red color) were averaged from all participants. Abbreviations: Exp1, experiment 1; Exp2, experiment 2; BOLD, blood oxygen level dependent.

**Table 1**

Summary of the averaged signal and its standard deviation over all participants for the fixation and visual stimulation blocks and the results of paired t-test between the two stimulation blocks at the selected brain areas for experiment 1.

ROIs	Methods	Fixation (f)	Visual (v)	P-value	$(S_v - S_f) * 100 / S_f$ (%)
PVC (BA 17)	BOLD	0.9938 $\pm 0.0018$	1.0059 $\pm 0.0017$	<0.0001	1.23 $\pm$ 0.36
	SEEPI_conductivity	0.9987 $\pm 0.0024$	1.0012 $\pm 0.0022$	0.073	0.24 $\pm$ 0.47
SVC (BA 18,19)	BOLD	0.9960 $\pm 0.0013$	1.0038 $\pm 0.0012$	<0.0001	0.79 $\pm$ 0.25
	SEEPI_conductivity	0.9978 $\pm 0.0016$	1.0020 $\pm 0.0015$	<b>0.0003</b>	0.43 $\pm$ 0.31
Cuneus	BOLD	0.9947 $\pm 0.0019$	1.0051 $\pm 0.0018$	<0.0001	1.04 $\pm$ 0.38
	SEEPI_conductivity	0.9976 $\pm 0.0024$	1.0023 $\pm 0.0023$	<b>0.0041</b>	0.47 $\pm$ 0.48
Lingual Gyrus	BOLD	0.9950 $\pm 0.0013$	1.0048 $\pm 0.0013$	<0.0001	1.01 $\pm$ 0.26
	SEEPI_conductivity	0.9995 $\pm 0.0019$	1.0005 $\pm 0.0018$	0.330	0.11 $\pm$ 0.38
PVC_CSF	BOLD	0.9919 $\pm 0.0051$	1.0081 $\pm 0.0051$	<0.0001	1.64 $\pm 1.04$
	SEEPI_conductivity	0.9956 $\pm 0.0113$	1.0044 $\pm 0.0113$	0.4709	0.91 $\pm 2.27$
SVC_CSF	BOLD	0.9936 $\pm 0.0025$	1.0064 $\pm 0.0025$	<0.0001	1.30 $\pm 0.52$
	SEEPI_conductivity	0.9914 $\pm 0.0094$	1.0086 $\pm 0.0094$	0.0879	1.75 $\pm 1.94$

$\frac{\Delta S}{S(\%)} = (\overline{S_v} - \overline{S_f}) \times 100\% / \overline{S_f}$ , in which  $\overline{S_v}$  and  $\overline{S_f}$  are the mean signal intensities during the visual (v) stimulation and fixation (f) conditions, respectively. Data are listed with mean  $\pm$  standard deviation averaged those values over 14 participants. The conductivity value was obtained from the MREPT technique of the multi-echo (me) spin-echo echo-planar-imaging (SEEPI) sequence.  $i_2 \times (i_1 > 0.5)$  PVC\_CSF and SVC\_CSF values were calculated with the signal from PVC or SVC ( $i_2$ ) multiplied by masking the cerebrospinal fluid (CSF) area for each participant ( $i_1$ ) and summarized those values to calculate mean  $\pm$  standard deviation over 14 participants.

The p-value indicates the result of a paired t-test of the mean value for each participant between fixation and visual stimulation tasks.

**Abbreviations:** region-of-interest (ROI); blood oxygen level-dependent (BOLD); primary visual cortex (PVC); secondary visual cortex (SVC); cerebrospinal fluid (CSF)

volume during stimulation (Geddes and Baker, 1967). However, in non-static conditions, blood dephased by the 180 pulse affects conductivity changes less than BOLD. Therefore, conductivity-based fMRI may better detect neuronal activities than BOLD fMRI. Additionally, neuronal stimulation causes cell swelling, altering intracellular and extracellular water content without changing high-frequency conductivity due to the relatively large voxel size (Lux et al., 1986). This study did not investigate the contribution of cell swelling effects on conductivity-based fMRI, necessitating further research.

#### 4.2. Contribution of CSF signals to conductivity changes during visual stimulation

One hypothesis of this study was that conductivity signals might change due to alterations in CSF signals during visual stimulation. However, our results showed that conductivity values were not significantly affected by CSF, as shown in Tables 1 and 2, and Fig. 4. We expected neural tissue to contain a substantial amount of highly conductive CSF components, which could contribute to changes in conductivity during stimulation. However, conductivity values at PVC\_CSF and SVC\_CSF were not significantly different between fixation and visual stimulations, indicating that conductivity changes during visual

**Table 2**

Summary of the averaged signal and its standard deviation over all participants for the fixation and visual stimulation blocks and the results of paired t-test between the two stimulation blocks at the selected brain areas for experiment 2.

ROIs	Methods	Fixation	Visual	P-value	$(S_v - S_f) * 100 / S_f$
PVC (BA 17)	BOLD	0.9985 $\pm 0.0007$	1.0014 $\pm 0.0007$	<0.0001	0.26 $\pm$ 0.14
	SEEPI_conductivity	0.9957 $\pm 0.0047$	1.0037 $\pm 0.0043$	<b>0.0025</b>	0.92 $\pm$ 1.02
SVC (BA 18,19)	bFFE_conductivity	0.9995 $\pm 0.0028$	1.0004 $\pm 0.0026$	0.698	0.06 $\pm$ 0.61
	BOLD	0.9994 $\pm 0.0008$	1.0006 $\pm 0.0007$	0.0153	0.11 $\pm$ 0.17
Cuneus	SEEPI_conductivity	0.9955 $\pm 0.0018$	1.0039 $\pm 0.0018$	<b>&lt;0.0001</b>	0.90 $\pm$ 0.35
	bFFE_conductivity	0.9999 $\pm 0.0023$	1.0001 $\pm 0.0021$	0.873	0.02 $\pm$ 0.44
Lingual Gyrus	BOLD	0.9992 $\pm 0.0009$	1.0008 $\pm 0.0009$	0.0053	0.14 $\pm$ 0.17
	SEEPI_conductivity	0.9965 $\pm 0.0032$	1.0034 $\pm 0.0031$	<b>0.0009</b>	0.67 $\pm$ 0.65
PVC_CSF	bFFE_conductivity	0.9992 $\pm 0.0023$	1.0007 $\pm 0.0021$	0.444	0.10 $\pm$ 0.51
	BOLD	0.9987 $\pm 0.0005$	1.0012 $\pm 0.0005$	<0.0001	0.22 $\pm$ 0.10
SVC_CSF	SEEPI_conductivity	0.9988 $\pm 0.0021$	1.0012 $\pm 0.0020$	<b>0.0378</b>	0.24 $\pm$ 0.41
	bFFE_conductivity	1.0000 $\pm 0.0043$	0.9993 $\pm 0.0040$	0.696	-0.08 $\pm$ 0.79
PVC_CSF	BOLD	0.9980 $\pm 0.0022$	1.002 $\pm 0.0022$	0.0029	0.3950 $\pm 0.4441$
	SEEPI_conductivity	0.9961 $\pm 0.0131$	1.003 $\pm 0.0132$	0.3302	0.6973 $\pm 2.6638$
SVC_CSF	bFFE_conductivity	0.9909 $\pm 0.0205$	1.0091 $\pm 0.0205$	0.0973	1.9126 $\pm 4.2732$
	BOLD	0.9991 $\pm 0.0024$	1.0009 $\pm 0.0024$	0.1693	0.1756 $\pm 0.4845$
PVC_CSF	SEEPI_conductivity	0.9966 $\pm 0.0063$	1.0024 $\pm 0.0065$	0.0898	0.5912 $\pm 1.3041$
	bFFE_conductivity	1.0006 $\pm 0.0094$	0.9980 $\pm 0.0071$	0.3453	-0.2554 $\pm 1.0742$

$\frac{\Delta S}{S(\%)} = (\overline{S_v} - \overline{S_f}) \times 100\% / \overline{S_f}$ , in which  $\overline{S_v}$  and  $\overline{S_f}$  are the mean signal intensities during the visual (v) stimulation and fixation (f) conditions, respectively. Data are listed with mean  $\pm$  standard deviation averaged those values over 16 participants. The conductivity values were obtained from the MREPT techniques of the single-echo spin-echo echo-planar-imaging (SEEPI) sequence (SEEPI\_conductivity) and the three-dimensional balanced fast-field-echo (bFFE) sequence (bFFE\_conductivity).

$i_2 \times (i_1 > 0.5)$  PVC\_CSF and SVC\_CSF values were calculated with the signal from PVC or SVC ( $i_2$ ) multiplied by masking the cerebrospinal fluid (CSF) area for each participant ( $i_1$ ) and summarized those values to calculate mean  $\pm$  standard deviation over 16 participants.

The p-value indicates the result of a paired t-test of the mean value for each participant between fixation and visual stimulation tasks.

**Abbreviations:** region-of-interest (ROI); blood oxygen level-dependent (BOLD); three-dimensional (3D) balanced fast-field-echo (bFFE); primary visual cortex (PVC); secondary visual cortex (SVC); cerebrospinal fluid (CSF)

stimulation may not be related to CSF changes in the visual cortex but rather to diffusion changes. A previous BOLD animal study showed decreased CSF volume in a voxel during visual stimulation (Jin and Kim, 2010). This change in the CSF volume fraction at the boundary of CSF and gray matter may alter the phase in the voxel, resulting in conductivity changes during visual stimulation. Our results also showed that BOLD signals changed at the PVC-CSF and SVC-CSF regions in experiment 1 (Table 1).

#### 4.3. Review of other findings related to conductivity-based fMRI

In this study, we used MREPT with SE-EPI and 3D bFFE sequences to

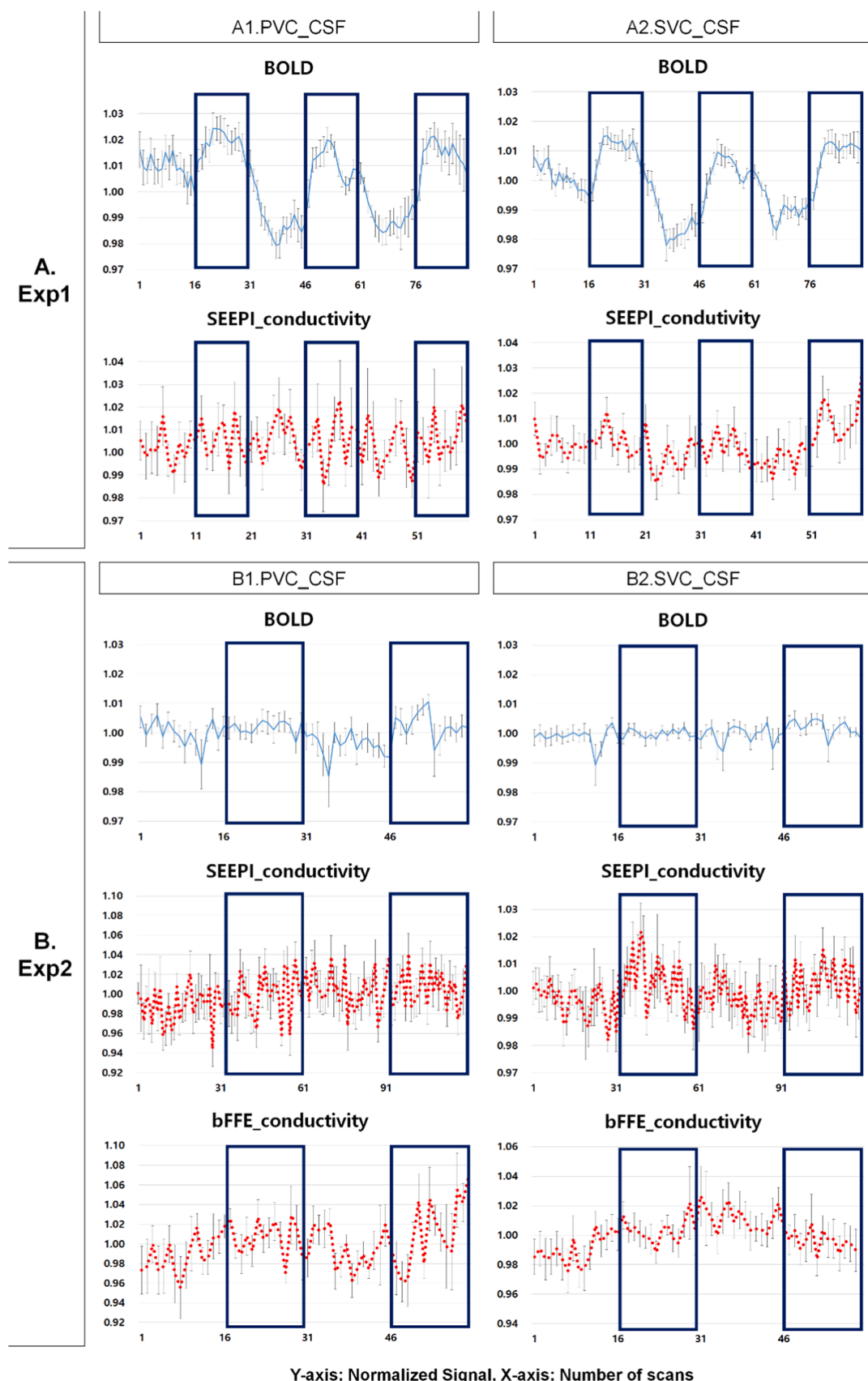


**Fig. 4.** Averaged signal changes over all participants during the visual stimulation for BOLD and MREPT with spin-echo echo-planar imaging (SEEPI) and three-dimensional balanced fast-field-echo (bFFE) for experiments 1 (A.Exp1) and 2 (B.Exp2) in the cerebrospinal fluid (CSF) areas at the primary visual cortex (PVC) and secondary visual cortex (SVC). The values of BOLD and conductivity (red color) were averaged from all participants. Abbreviations: Exp1, experiment 1; Exp2, experiment 2; BOLD, blood oxygen level dependent.

map conductivities during visual stimulation. Our findings indicate that the activation map was more visible with SE-EPI than bFFE. Any imaging sequence can map phase. MREPT signals are typically acquired using spin-echo or gradient-echo sequences to obtain both magnitude and phase information. The bFFE sequence is highly sensitive to small off-resonance phase changes (Bieri et al., 2006; Lee et al., 2016). However, we did not observe this advantage with the bFFE sequence in this study. Activation patterns differed between sequences due to varying noise and sensitivity to neuronal signal changes. SE-EPI provided a more stable conductivity map, suggesting it may be better for MREPT-based fMRI, but further studies are needed for comparison and optimization.

During visual stimulation, we predominantly observed increased conductivity in most participants, suggesting that visual stimulation generally leads to heightened neural and hemodynamic activity, which correlates with increased ion concentration and mobility, thereby increasing conductivity. However, we also detected decreased conductivity in some voxels in certain participants (Supplementary Figure S6). The reasons for decreased conductivity during stimulation are not fully understood. One possible explanation is that decreased activity in certain visual cortex regions may reflect inhibitory processes or reduced synaptic activity, leading to decreased ion mobility and hence reduced conductivity. Additionally, not all participants' brains respond uniformly to visual stimuli, leading to variability in conductivity changes. Differences in participants' baseline conductivity levels could also result in apparent decreases in some voxels, depending on their initial state and how their brains adapt to the visual stimulus. Furthermore, decreased conductivity might result from localized hemodynamic changes, such as reduced blood flow or volume in specific brain regions, impacting the local ionic environment. Variability in the measurement process, including noise and artifacts, could also contribute to the observed decreases in conductivity in certain voxels. Therefore, further studies are required to investigate the process of deactivation with MREPT fMRI.

Conductivity-based fMRI can be performed with MREIT and MREPT, although the activation results depend on the contribution of cellular compartments. MREPT-based fMRI is simpler than MREIT-based fMRI due to fewer phase-encoding steps and less complex reconstruction. MREIT-based fMRI may be advantageous at lower frequencies (<100 Hz), aligning with physiological local field potentials, though some studies did not show frequency-dependent conductivity changes (Gabriel et al., 2009; Logothetis et al., 2007; Miceli et al., 2017; Nelson et al., 2013; Nicholson and Sykova, 1998; Sadleir et al., 2017). MREIT imaging currents can affect active tissue spiking, unlike MREPT. MREIT-based fMRI offers higher functional SNR due to injected currents amplifying phase changes. Prior studies have shown changes in cell conductivity with neural activity using MREIT, but no such studies exist for MREPT. A previous EIT study showed an increase of 0.5–1.0 % in raw voltages during visual-evoked responses in healthy volunteers (Sadleir et al., 2019, 2017; Tidswell et al., 2001). In vitro MREIT studies have shown changes in cell conductivity caused by neural activity with the injection of electrical current (Miceli et al., 2017; Sadleir et al., 2019, 2017). In vivo MREIT studies have shown increased conductivity during visual-evoked responses in healthy volunteers (Tidswell et al., 2001), in monkeys (Logothetis et al., 2007), in cats (Wagner et al., 2014), and in rat (Dowrick et al., 2015). Although there have been several MREIT-based fMRI studies, there have not been many MREPT experiments on the detection of neural activity with multiple sequences. Future research should explore MREPT's potential to detect neuronal electrical activity and hemodynamic changes.

The permittivity ( $\epsilon H$ ) is the inverse of conductivity ( $1/\sigma H$ ). In this study, we did not look at the permittivity changes during the visual stimulation because the interpretation of permittivity changes ( $1/\sigma H$ ) is much more complicated than conductivity changes. We can expect that permittivity can be changed during the visual stimulation because conductivity was changed. However, we cannot say which one is more sensitive to response to visual stimulation. Therefore, further study

should be necessary to investigate the functional response of both conductivity and permittivity during visual stimulation.

For fMRI studies, people have used the minimum number of participants 5 (Desmond and Glover, 2002; Szucs and Ioannidis, 2020). Of course, many subjects are better for concluding the overall results. We thought that 30 participants were enough to demonstrate the feasibility of a novel MREPT-based fMRI method to measure neuronal activity changes during visual stimulation in the human brain.

#### 4.4. Limitations

This study had several limitations. First, we used the same voxel size for both BOLD and MREPT to compare fMRI signals between the two methods. A spatial resolution is typically critical for measuring spin phases of MREPT in the voxel. A high voxel size of MREPT can average the imaging phase in a voxel. With a relatively large voxel size of MREPT, our data may not be representative of direct evaluation of neuronal activity. It may therefore be necessary to acquire functional MREPT data with a relatively high resolution, although the signal-to-noise ratio can be reduced. Second, we used a relatively long TR for the SE-EPI: TR of 3 s with a single echo and TR of 6 s with the two echoes. Those TR values were relatively long, and the temporal resolution to obtain sequential imaging was poor. Therefore, it may be better to apply a short TR such as 1 s or even 0.5 s. Further, TEs of 30 and/or 80 ms for SE-EPI may be too long to obtain optimum phase changes. However, a shorter TE may not show a good BOLD response. Therefore, further research is needed to optimize TE to obtain a good phase map. Third, in this study, we did not directly compare the effect of physiological noise in MREPT-based fMRI data. The activation with removing physiological noise was reduced compared to without removing physiological noise. Physiological noises such as the cardiac and respiratory signals are a major confounder for fMRI data. Those noise signals also contributed to the conductivity signals of MREPT. Therefore, future studies should further investigate the relationship between MREPT signals and physiological fluctuation signals. Finally, the proposed functional MREPT reconstruction procedure using a relatively short MR scan duration suffers from interfering noise and undesired artifacts in the reconstructed conductivity map due to weak phase signals and defective regions. Therefore, to increase the sensitivity for neuronal activity, functional MREPT requires further optimization of signal acquisitions.

#### 5. Conclusion

Conductivity-based fMRI would be based on due to the alteration of ion concentrations and mobilities. The conductivity value was very little increased during the visual stimulation in visual cortex areas, but was much weaker than BOLD. The conductivity change during the visual stimulation was less than 1 % compared to that in the fixation block. Conductivity values at PVC-CSF and SVC-CSF were not significantly different between fixation and visual stimulations, indicating that the conductivity changes during the visual stimulation may be not related to CSF changes in the visual cortex and may be related to the mobility of charged ions under the influence of electric field changes. It is unclear whether the slight changes of conductivity in the brain during functional activity were due to true physiological mechanisms. The potential for imaging electrical activity in the brain would potentially be useful in several neurophysiological studies. Future research should explore MREPT's potential to detect neuronal electrical activity and hemodynamic changes with further optimization of an MREPT technique.

#### Ethics statement

The studies involving human participants were reviewed and approved by Kyung Hee University Hospital at Gangdong Institutional Review Board (IRB KHNC 2020-03-017). The participants provided

their written informed consent to participate in this study.

## Funding

The research was supported by the National Research Foundation of Korea (NRF) grants funded by the Ministry of Science and ICT (2020R1A2C1004749, G.H.J.; RS-2024-00335770, G.H.J; 2019R1A2C1004660, O.I.K.; RS-2023-00250977, M.L.), Republic of Korea

## CRediT authorship contribution statement

**Mun Bae Lee:** Writing – review & editing, Writing – original draft, Software, Methodology, Formal analysis. **Jeongin Jeong:** Writing – review & editing, Visualization, Software, Formal analysis. **Hyug-Gi Kim:** Writing – review & editing, Writing – original draft, Visualization, Formal analysis, Data curation. **Youngeun Yoon:** Writing – review & editing, Visualization, Software, Methodology, Formal analysis. **Oh In Kwon:** Writing – review & editing, Validation, Supervision, Methodology. **Geonho Jahng:** Writing – review & editing, Writing – original draft, Visualization, Validation, Supervision, Resources, Project administration, Methodology, Investigation, Funding acquisition, Formal analysis, Data curation, Conceptualization. **Jiyoonee Lee:** Writing – review & editing, Visualization, Software, Formal analysis.

## Declaration of Competing Interest

The authors declare that the research was conducted in the absence of any commercial or financial relationships that could be construed as a potential conflict of interest.

## Data availability

Data will be made available on request.

## Appendix A. Supporting information

Supplementary data associated with this article can be found in the online version at [doi:10.1016/j.jneumeth.2024.110288](https://doi.org/10.1016/j.jneumeth.2024.110288).

## References

- Althubeati, S., Avery, A., Tench, C.R., Lobo, D.N., Salter, A., Eldeghaidy, S., 2022. Mapping brain activity of gut-brain signaling to appetite and satiety in healthy adults: A systematic review and functional neuroimaging meta-analysis. *Neurosci. Biobehav. R.* 136.
- Bieri, O., Maderwald, S., Ladd, M.E., Scheffler, K., 2006. Balanced alternating steady-state elastography. *Magn. Reson. Med.* 55, 233–241.
- Buxton, R.B., Frank, L.R., 1997. A model for the coupling between cerebral blood flow and oxygen metabolism during neural stimulation. *J. Cereb. Blood Flow. Metab.* 17, 64–72.
- Celeghin, A., Palermo, S., Giampaolo, R., Di Fini, G., Gandino, G., Civillotti, C., 2023. Brain correlates of eating disorders in response to food visual stimuli: a systematic narrative review of fMRI studies. *Brain Sci.* 13.
- Chaudhry, A.A., Naim, S., Gul, M., Chaudhry, A., Chen, M., Jandial, R., Badie, B., 2021. Utility of preoperative blood-oxygen-level-dependent functional MR imaging in patients with a central nervous system Neoplasm. *Neuroimag. Clin. N. Am.* 31, 93–102.
- Collins, C.M., Yang, B., Yang, Q.X., Smith, M.B., 2002. Numerical calculations of the static magnetic field in three-dimensional multi-tissue models of the human head. *Magn. Reson Imaging* 20, 413–424.
- Desmond, J.E., Glover, G.H., 2002. Estimating sample size in functional MRI (fMRI) neuroimaging studies: Statistical power analyses. *J. Neurosci. Meth.* 118, 115–128.
- Dowrick, T., Blochet, C., Holder, D., 2015. In vivo bioimpedance measurement of healthy and ischaemic rat brain: implications for stroke imaging using electrical impedance tomography. *Physiol. Meas.* 36, 1273–1282.
- Friston, K.J., Worsley, K.J., Frackowiak, R.S., Mazziotta, J.C., Evans, A.C., 1994. Assessing the significance of focal activations using their spatial extent. *Hum. Brain Mapp.* 1, 210–220.
- Gabriel, C., Peyman, A., Grant, E.H., 2009. Electrical conductivity of tissue at frequencies below 1 MHz. *Phys. Med. Biol.* 54, 4863–4878.
- Geddes, L.A., Baker, L.E., 1967. The specific resistance of biological material—a compendium of data for the biomedical engineer and physiologist. *Med. Biol. Eng.* 5, 271–293.
- Gurler, N., Ider, Y.Z., 2017. Gradient-based electrical conductivity imaging using MR phase. *Magn. Reson. Med.* 77, 137–150.
- Hancu, I., Liu, J., Hua, Y., Lee, S.K., 2019. Electrical properties tomography: Available contrast and reconstruction capabilities. *Magn. Reson. Med.* 81, 803–810.
- Hancu, I., Roberts, J.C., Bulumulla, S., Lee, S.K., 2015. On conductivity, permittivity, apparent diffusion coefficient, and their usefulness as cancer markers at MRI frequencies. *Magn. Reson. Med.* 73, 2025–2029.
- Heeger, D.J., Huk, A.C., Geisler, W.S., Albrecht, D.G., 2000. Spikes versus BOLD: what does neuroimaging tell us about neuronal activity? *Nat. Neurosci.* 3, 631–633.
- Hense, K., Plank, T., Wendt, C., Dodoo-Schittko, F., Burnes, E., Greene, M.W., Schmidt, N.O., Proescholdt, M., Rosengarth, K., 2021. fMRI retinotopic mapping in patients with brain tumors and space-occupying brain lesions in the area of the occipital lobe. *Cancers* 13.
- Huang, S., Shao, W., Wang, M.L., Zhang, D.Q., 2021. fMRI-based decoding of visual information from human brain activity: a brief review. *Int. J. Autom. Comput.* 18, 170–184.
- Jahng, G.H., Lee, M.B., Kim, H.J., Je Woo, E., Kwon, O.I., 2021. Low-frequency dominant electrical conductivity imaging of *in vivo* human brain using high-frequency conductivity at Larmor-frequency and spherical mean diffusivity without external injection current. *Neuroimage* 225, 117466.
- Jin, T., Kim, S.G., 2010. Change of the cerebrospinal fluid volume during brain activation investigated by T1rho-weighted fMRI. *Neuroimage* 51, 1378–1383.
- Katscher, U., Kim, D.H., Seo, J.K., 2013. Recent progress and future challenges in MR electric properties tomography. *Comput. Math. Methods Med.* 2013, 546562.
- Katscher, U., van den Berg, C.A.T., 2017. Electric properties tomography: Biochemical, physical and technical background, evaluation and clinical applications. *NMR Biomed.* 30.
- Katscher, U., Voigt, T., Findeklee, C., Vernickel, P., Nehrke, K., Dossel, O., 2009. Determination of electric conductivity and local SAR via B1 mapping. *IEEE Trans. Med. Imaging* 28, 1365–1374.
- Konn, D., Gowland, P., Bowtell, R., 2003. MRI detection of weak magnetic fields due to an extended current dipole in a conducting sphere: a model for direct detection of neuronal currents in the brain. *Magn. Reson. Med.* 50, 40–49.
- Kotoula, V., Evans, J.W., Punturi, C.E., Zarate, C.A., Jr, 2023. Review: The use of functional magnetic resonance imaging (fMRI) in clinical trials and experimental research studies for depression. *Front. Neuroimaging* 2, 1110258.
- Kwong, K.K., Belliveau, J.W., Chesler, D.A., Goldberg, I.E., Weisskoff, R.M., Poncelet, B.P., Kennedy, D.N., Hoppel, B.E., Cohen, M.S., Turner, R., et al., 1992. Dynamic magnetic resonance imaging of human brain activity during primary sensory stimulation. *Proc. Natl. Acad. Sci. USA* 89, 5675–5679.
- Lakhani, D.A., Sabsevitz, D.S., Chaichana, K.L., Quinones-Hinojosa, A., Middlebrooks, E.H., 2023. Current state of functional MRI in the presurgical planning of brain tumors. *Radiol-Imag. Cancer* 5.
- Le Bihan, D., Urayama, S., Aso, T., Hanakawa, T., Fukuyama, H., 2006. Direct and fast detection of neuronal activation in the human brain with diffusion MRI. *Proc. Natl. Acad. Sci. USA* 103, 8263–8268.
- Lee, H., Jeong, W.C., Kim, H.J., Woo, E.J., Park, J., 2016. Alternating steady state free precession for estimation of current-induced magnetic flux density: A feasibility study. *Magn. Reson. Med.* 75, 2009–2019.
- Leijesen, R., Brink, W., van den Berg, C., Webb, A., Remis, R., 2021. Electrical properties tomography: a methodological review. *Diagn. (Basel)* 11.
- Logothetis, N.K., Kayser, C., Oeltermann, A., 2007. In vivo measurement of cortical impedance spectrum in monkeys: implications for signal propagation. *Neuron* 55, 809–823.
- Logothetis, N.K., Pauls, J., Augath, M., Trinath, T., Oeltermann, A., 2001. Neurophysiological investigation of the basis of the fMRI signal. *Nature* 412, 150–157.
- Luo, Q., Lu, H., Lu, H., Sensemam, D., Worsley, K., Yang, Y., Gao, J.H., 2009. Physiologically evoked neuronal current MRI in a bloodless turtle brain: detectable or not? *Neuroimage* 47, 1268–1276.
- Lux, H.D., Heinemann, U., Dietzel, I., 1986. Ionic changes and alterations in the size of the extracellular space during epileptic activity. *Adv. Neurol.* 44, 619–639.
- Meng, L., Ge, K., 2022. Decoding visual fMRI stimuli from human brain based on graph convolutional neural network. *Brain Sci.* 12.
- Miceli, S., Ness, T.V., Einevoll, G.T., Schubert, D., 2017. Impedance spectrum in cortical tissue: implications for propagation of lfp signals on the microscopic level. *eNeuro* 4.
- Nelson, M.J., Bosch, C., Venance, L., Pouget, P., 2013. Microscale inhomogeneity of brain tissue distorts electrical signal propagation. *J. Neurosci.* 33 (7), 2821.
- Nicholson, C., Sykova, E., 1998. Extracellular space structure revealed by diffusion analysis. *Trends Neurosci.* 21, 207–215.
- Ogawa, S., Tank, D.W., Menon, R., Ellermann, J.M., Kim, S.G., Merkle, H., Ugurbil, K., 1992. Intrinsic signal changes accompanying sensory stimulation: functional brain mapping with magnetic resonance imaging. *Proc. Natl. Acad. Sci. USA* 89, 5951–5955.
- Park, J., Soucy, E., Segawa, J., Mair, R., Konkle, T., 2024. Immersive scene representation in human visual cortex with ultra-wide-angle neuroimaging. *Nat. Commun.* 15.
- Sadleir, R.J., Fu, F., Chauhan, M., 2019. Functional magnetic resonance electrical impedance tomography (fMREIT) sensitivity analysis using an active bidomain finite-element model of neural tissue. *Magn. Reson. Med.* 81, 602–614.
- Sadleir, R.J., Fu, F., Falgas, C., Holland, S., Bogges, M., Grant, S.C., Woo, E.J., 2017. Direct detection of neural activity *in vitro* using magnetic resonance electrical impedance tomography (MREIT). *Neuroimage* 161, 104–119.

- Soares, J.M., Magalhaes, R., Moreira, P.S., Sousa, A., Ganz, E., Sampaio, A., Alves, V., Marques, P., Sousa, N., 2016. A Hitchhiker's guide to functional magnetic resonance imaging. *Front. Neurosci. -Switz.* 10.
- Szucs, D., Ioannidis, J.P.A., 2020. Sample size evolution in neuroimaging research: An evaluation of highly-cited studies (1990-2012) and of latest practices (2017-2018) in high-impact journals. *Neuroimage* 221.
- Tidswell, T., Gibson, A., Bayford, R.H., Holder, D.S., 2001. Three-dimensional electrical impedance tomography of human brain activity. *Neuroimage* 13, 283–294.
- Truong, T.K., Wilbur, J.L., Song, A.W., 2006. Synchronized detection of minute electrical currents with MRI using Lorentz effect imaging. *J. Magn. Reson.* 179, 85–91.
- Turner, R., 2002. How much cortex can a vein drain? Downstream dilution of activation-related cerebral blood oxygenation changes. *Neuroimage* 16, 1062–1067.
- Wagner, T., Eden, U., Rushmore, J., Russo, C.J., Dipietro, L., Fregni, F., Simon, S., Rotman, S., Pitskel, N.B., Ramos-Estebanez, C., Pascual-Leone, A., Grodzinsky, A.J., Zahn, M., Valero-Cabre, A., 2014. Impact of brain tissue filtering on neurostimulation fields: a modeling study. *Neuroimage* 85 (Pt 3), 1048–1057.
- Wittkuhn, L., Schuck, N.W., 2021. Dynamics of fMRI patterns reflect sub-second activation sequences and reveal replay in human visual cortex. *Nat. Commun.* 12.